ACS Catalysis

pubs.acs.org/acscatalysis

Research Article

# Computational-Aided Engineering of a Selective Unspecific Peroxygenase toward Enantiodivergent β-Ionone Hydroxylation

Judith Münch,[#] Jordi Soler,[#] Nicole Hünecke, Dominik Homann, Marc Garcia-Borràs,* and Martin J. Weissenborn*

Cite This: *ACS Catal.* 2023, 13, 8963−8972

Read Online

ACCESS | Metrics & More | Article Recommendations | Supporting Information

**ABSTRACT:** Unspecific peroxygenases (UPOs) perform oxyfunctionalizations for a wide range of substrates utilizing $H_2O_2$ without the need for further reductive equivalents or electron transfer chains. Tailoring these promising enzymes toward industrial application was intensely pursued in the last decade with engineering campaigns addressing the heterologous expression, activity, stability, and improvements in chemo- and regioselectivity. One hitherto missing integral part was the targeted engineering of enantioselectivity for specific substrates with poor starting enantioselectivity. In this work, we present the engineering of the short-type *Mth*UPO toward the enantiodivergent hydroxylation of the terpene model substrate, β-ionone. Guided by computational modeling, we designed a small smart library and screened it with a GC−MS setup. After two rounds of iterative protein evolution, the activity increased up to 17-fold and reached a regioselectivity of up to 99.6% for the 4-hydroxy-β-ionone. Enantiodivergent variants were identified with enantiomeric ratios of 96.6:3.4 (*R*) and 0.3:99.7 (*S*), respectively.

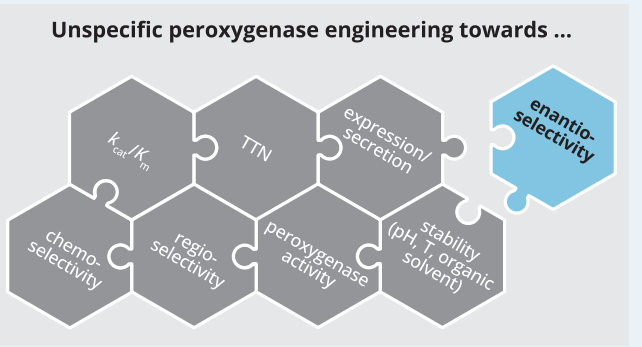


**KEYWORDS:** *directed evolution, unspecific peroxygenase, terpenes, hydroxylation, β-ionone, computational-guided protein engineering*



## INTRODUCTION

Oxyfunctionalyzation reactions are of tremendous importance in the field of synthetic chemistry, as they give access to new synthetic strategies, especially in late-stage functionalizations of complex molecules.[1] Nature offers an abundance of enzymes for catalyzing oxyfunctionalization reactions.[2,3] The most prominent and well-known class of enzymes in this field are the cytochrome P450 monooxygenases (P450s). P450s display a huge versatility of substrate-binding pockets and, thus, a tremendous substrate scope while maintaining high selectivity.[3,4] Two decades ago, a new enzyme class with similar properties emerged: the unspecific peroxygenases (UPOs) with fungal origin.[5−7] UPOs are inherently stable, secreted enzymes that catalyze reactions outside the regulated cell environment.[6] In contrast to P450s, they do not utilize molecular oxygen but hydrogen peroxide, in which the oxygen is already pre-reduced. This averts the necessity of cofactors such as NAD(P)H and a complex electron transport chain. Limited access to protocols for UPO production was formerly a huge drawback. Recent work gave access to the heterologous production of UPOs in fast-growing host organisms using protein engineering,[7] signal peptide,[8] and promoter shuffling.[9]

Engineering efforts at the mature protein led to UPO variants with improved peroxygenase/peroxidase ratios;[10] increases in activity (TON and $k_{cat}/K_m$);[11] improvements in thermo-,[12] pH-,[13] and solvent-stabilities;[12] and shifts in chemo- and regioselectivities.[10,14−16] Contrary to what their name suggests, UPOs often inherently exhibit excellent chemo-, regio-, and enantioselectivities for a range of substrates.[17] However, the engineering of UPOs for the oxyfunctionalization of specific substrates with initially poor enantioselectivities in a targeted manner remained elusive. A recent untargeted approach using the FuncLib algorithm led to impressive shifts in enantioselectivity.[18]

Our objective was to address the existing limitations and demonstrate the successful engineering of a UPO toward the enantioselective conversion of a selected substrate with low inherent enantioselectivity.

Particularly challenging targets for enantioselectivity engineering are terpenes and terpenoids. They are the largest group of natural products with approximately 80,000 different reported structures.[19] They occur mainly as secondary plant metabolites and display outstanding pharmacological bio-

Received: February 14, 2023
Revised: May 17, 2023
Published: June 21, 2023





https://doi.org/10.1021/acscatal.3c00702
*ACS Catal.* 2023, 13, 8963−8972

**Scheme 1. Enzymatic Hydroxylation of β-Ionone**

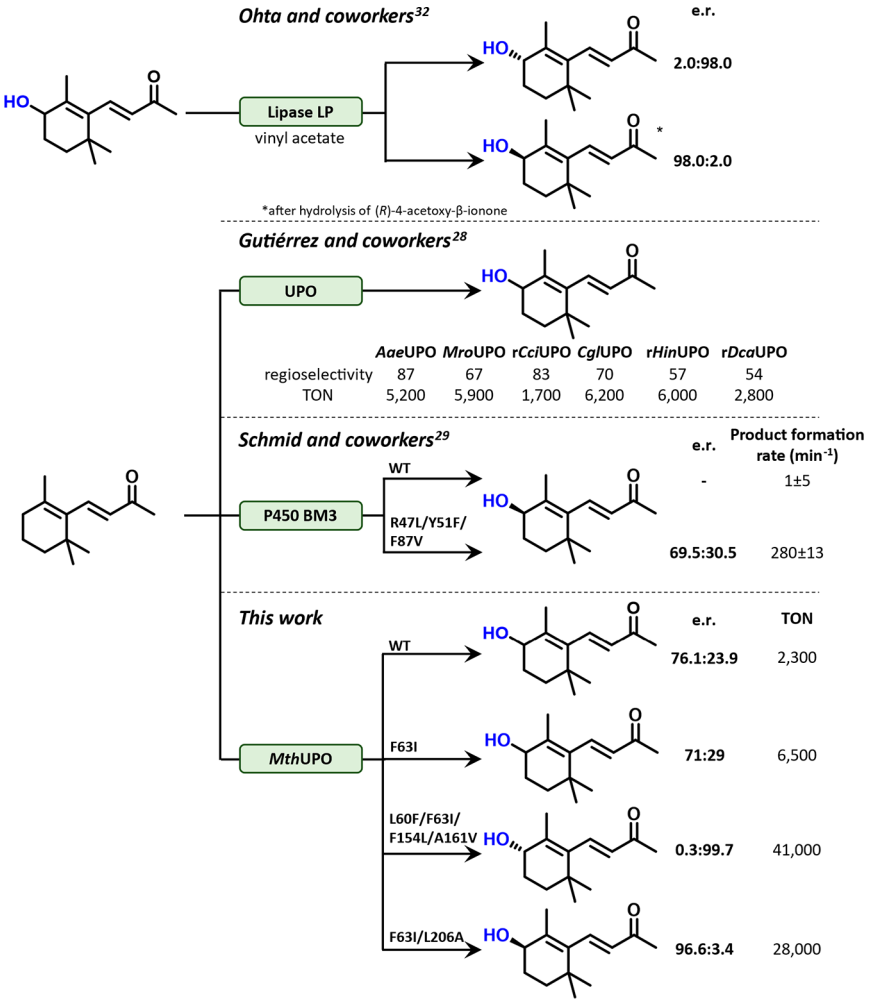


activity, making them attractive for medical and chemical industries. Their great structural diversity offers many opportunities for different regio- and enantioselective oxyfunctionalization reactions.

There have been several impressive engineering efforts of P450s toward terpenes and steroids. The engineering of $P450_{BM3}$ was demonstrated toward the enantiodivergent hydroxylation of five different steroid substrates with selectivity values between e.r. of 14:86 and 0:100. The variants showing this significant improvement in enantioselectivity were obtained through a directed evolution campaign with three rounds of CASTing. The library design was, hereby, based on molecular dynamics (MD) simulations and mutability landscaping.[20] Another work reported the engineering of $P450_{BM3}$ toward the regio- and stereoselective hydroxylation of the diterpenoid β-cembrenediol. The engineering campaign was based on the insertion of rational mutants and three sequential rounds of site saturation mutagenesis. The obtained variants were able to hydroxylate the C9 and C10 position, respectively, with regioselectivities up to 100% and a diastereomeric ratio of 89:11 for C9 and 74:26 for C10.[21]

One interesting group of terpenoids are ionones—also known as rose ketones. They are highly valued compounds in the fragrance industry; the annual production of β-ionone amounts to 4000−8000 tons.[22] They further function as building blocks for the synthesis of many carotenoids and retinol (vitamin A).[23] Numerous pharmacological effects are described for ionones and their derivatives including anticancer, chemopreventive, cancer-promoting, melanogenesis, anti-inflammatory, and antimicrobial actions.[24] 3-hydroxy-β-ionone displays anti-cancer properties inhibiting progression and inducing apoptosis of SCC15 cells.[25] 5,6-epoxy-β-ionone inhibits the tumor-promoting agent 12-O-tetradecanoylphorbol-13-acetate (TPA) even more effectively compared to parent compound β-ionone.[26] 4-Hydroxy-β-ionone derivatives proved to be potent inhibitors of prostate cancer cell proliferation (LNCaP, MDA-PCa-2b, C4-2B, and 22Rv1) and full antagonists of the wild-type androgen receptor (AR) and various clinically important mutated ARs.[27]

Initial studies on the enzymatic oxyfunctionalization of β-ionone have been carried out (Scheme 1). The hydroxylation of α- and β-ionone performed by several UPOs led to a diverse range of hydroxylation and epoxidation products.[28] The hydroxylation of β-ionone has also been pursued using various P450s.[29−31] First, P450 engineering efforts showed an up to 280-fold increased product formation rate toward α- and β-ionone hydroxylations, however, enhancing the enantioselectivity proved challenging.[29] Enantioselective 4-hydroxy-β-ionone formation has been achieved both through enzymatic kinetic resolution[32] and by CYP2B6, which was recombinantly expressed in *Trichoplusia ni* cells.[31]


https://doi.org/10.1021/acscatal.3c00702
ACS Catal. 2023, 13, 8963−8972

Scheme 2. β-Ionone (1) Oxygenation by wt *Mth*UPO Showing the Different Oxygenated Derivatives[a]

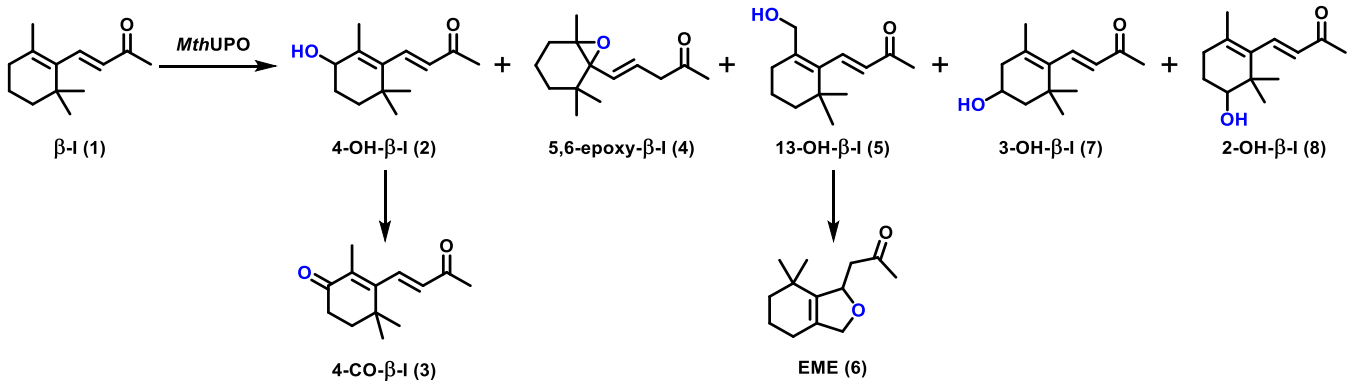


[a]the regioselective distribution of the products for different enzyme variants can be found in Table S9.

With the maturation of computational modeling methods for the study of biocatalysts, new avenues are opening up for the generation of ever smaller and more intelligent protein library designs.[33]

In the present work, we engineered new UPO variants to enantioselectively access C4 hydroxylated stereoisomers of β-ionone. We applied a computational-aided engineering approach based on substrate-bound (restrained-) MD simulations to explore near-attack conformations (NACs) of the selective hydroxylation and characterized relevant binding modes of the model substrate β-ionone. This led to the identification of relevant residues for the substrate positioning and, hence, the design of a small smart library to alter the active site pocket of *Mth*UPO. In this way, we could direct the selectivity of the oxyfunctionalization toward enantioselective *R*/*S* C4 hydroxylation. The screening was performed by the previously developed multiple injection in a single experimental run (MISER) GC−MS method[14,16,34] focusing on activity increase. In the MISER setup, 96 samples are injected into the GC within one experimental run. Product quantifications are performed solely in the MS via different *m*/*z* ratios without the need for substrate/product separation, allowing an injection frequency of up to 30 s and, hence, a GC analysis of one microtiter plate within 48 min. The best variants were rescreened with a chiral GC−MS to determine enantioselectivities. This enabled the engineering of two highly active and enantiodivergent *Mth*UPO variants for (*R*/S)-4-hydroxy-β-ionone formation in two rounds of computationally guided enzyme evolution.

## RESULTS AND DISCUSSION

**Identification of the β-Ionone Hydroxylating UPO *Mth*UPO.** We commenced with a pre-screening of five UPO enzymes to determine starting activities and selectivities, thereby, focusing on hydroxylation over epoxidation reactions (Table S4). We selected *Mth*UPO as an enzyme, as it displayed a regioselectivity of 88% for the main hydroxylation at the C4 position yielding 4-hydroxy-β-ionone (2), and a turnover number (TON) of approximately 2300. Further side products were β-ionone-5,6-epoxide (5,6-epoxy-β-I, 4), 7,11-epoxymegastigma-5(6)-en-9-one (EME, 6), 2-hydroxy-β-ionone (2-OH-β-I, 8), and 3-hydroxy-β-ionone (3-OH-β-I, 7, Scheme 2). Wild-type (wt) *Mth*UPO reached an enantiomeric ratio of 76:24 with a preference for (*R*)-4-hydroxy-β-ionone (2).

**Development of an Engineering Strategy Based on Computational Modeling.** The screening of different variants is often the most time-consuming step within a directed evolution campaign. Refined methods for creating small and smart mutant libraries have been developed to address this issue, including the combinatorial active-site saturation test (CAST),[35,36] iterative saturation mutagenesis (ISM),[37] or focused rational iterative site-specific mutagenesis (FRISM).[38] Inspired by these strategies, we utilized a computational-aided directed evolution strategy. This approach combined *in silico* analysis and experimental screening using the MISER GC−MS method.[14,16,34] The final aim was to engineer enantiodivergent enzyme variants that allow the selective formation of (*R*/*S*)-4-hydroxy-β-ionone products.

An accurate computational protein model was generated to reproduce the experimental observations for wt *Mth*UPO-catalyzed oxyfunctionalization of β-ionone. We combined density functional theory (DFT) calculations and MD simulations to characterize its reactivity pattern. DFT calculations were carried out using a truncated model, which includes the heme pyrrole core, a methyl thiolate to mimic the Cys axial ligation, and the β-ionone substrate (see Supporting Information for details). These data served to explore the intrinsic reactivity of β-ionone toward heme compound I. The transition states (TSs) were modeled for epoxidations and C−H activations of all non-equivalent C−H positions. The C−H activation was modeled as a hydrogen-atom transfer (HAT), which corresponds to the rate-limiting step of the hydroxylation reaction. As expected, calculations indicated that the epoxidation at cyclic double bond is energetically more favorable than the HAT C−H activation at the vinylic C4 position by only a few kcal·mol$^{-1}$ (Figures 1 and S2). Other inactivated C−H positions exhibit higher HAT barriers.

To assess the accessible catalytically relevant binding modes of the substrate when bound in the active site and to study the catalyst control exerted by the enzyme considering its conformational landscape, we performed MD simulations with the β-ionone bound in wt *Mth*UPO's active site. The MD simulations in this step were performed using a previously generated computational model of wt *Mth*UPO.[14] Optimal geometric parameters required for C−H activation via HAT and epoxidation were taken from DFT model-optimized TSs (Figures S3 and S4).

MD simulations with the bound substrate indicated that β-ionone can explore NACs that could effectively lead to C−H activation via HAT at C4, C2, C10, C11, and C12 positions (Figures S3 and S4). The epoxidation conformations, however, barely explored NACs.



https://doi.org/10.1021/acscatal.3c00702
ACS Catal. 2023, 13, 8963−8972

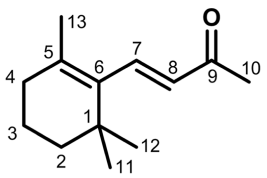


| Structure | ΔG‡ |
|---|---|
| TS C5 epoxidation (q) | 18.5 |
| TS C8 epoxidation (d) | 20.1 |
| TS C2-HAT (q) | 24.2 |
| TS C3-HAT (q) | 26.3 |
| TS C4-HAT (d) | 19.4 |
| TS C10-HAT (q) | 25.8 |
| TS C11/12-HAT (q) | 30.9 |
| TS C13-HAT (d) | 20.3 |

**Figure 1.** Intrinsic reactivity of *β*-ionone explored using a truncated computational model ("*theozyme*", i.e., theoretical enzyme). DFT calculated C−H activation via HAT and epoxidation TSs for all non-equivalent positions of *β*-ionone. Epoxidation of the cyclic double bond and *α*,*β*-alkene and hydroxylations at vinylic C4 (cyclic) and C13 (methyl) positions are intrinsically the most favored oxidation of *β*-ionone in the absence of any catalyst control. See Figure S2 for additional details. Energies are given in kcal·mol$^{-1}$.

Even though the C−O bond formation at C5 leading to epoxide formation is energetically preferred over the HAT at the C4 position (DFT optimized lowest TS, Figure 1), we experimentally observed only scarce amounts of epoxide product formation (Table S9).

This is in agreement with the fact that the C−O bond formation TS requires a very tight approach of the substrate to the catalytic Fe═O moiety (TS C5 epoxidation, Figure 2). This required NAC for epoxidation is sterically hindered in the active site of *Mth*UPO and cannot be efficiently explored by *β*-ionone—as revealed by MD simulations. On the other hand, the NAC required for C4 HAT is easily accessible for *β*-ionone (TS C4-HAT, Figures 2 and S5). This leads to a hampered epoxide formation while binding modes that allow the energetically most favored hydroxylation at position C4 are easily explored.

Taking all this together, computations described the catalyst control exerted by the wt *Mth*UPO on the selectivity oxyfunctionalization of *β*-ionone, reproducing the experimental observations, and provided a sound model to serve as the starting point for our semi-rational engineering strategy.

We attempted to improve our starting activity before focusing on shifting the enantioselectivity by screening an in-house *Mth*UPO library, which was obtained during a previous enzyme engineering campaign toward NBD hydroxylation (Figure S6). The most active variant F63I was selected as the parent variant for the engineering campaign displaying a 4.5-fold higher product formation rate than wt *Mth*UPO with similar regio- and enantioselectivities.

To restrict the accessible binding modes of *β*-ionone and, thus, control the stereoselectivity of the C4 hydroxylation, we aimed to design focused libraries based on computational predictions. To identify positions for the mutagenesis, MD simulations were performed with *Mth*UPO F63I in which *β*-ionone is forced to explore NACs for an effective C4−H HAT, mimicking DFT model TSs geometries (Figure 3A). Geometric restraints were included during the MD trajectories (restrained-MD simulations) in which the pro-*R* or pro-*S* C4−H positions—in independent trajectories—were forced to be at short distance to the Fe-oxo catalytic species (Figure 3A, see Supporting Information for details). These restrained-MD simulations provided structural descriptions of the arrangement of the active site that is required for accommodating *β*-ionone in a pro-R and pro-S NAC, respectively (Figure 3B). It is crucial to acknowledge that *Mth*UPO F63I already demonstrated the ability to catalyze C4−H activations, although the efficiency was limited, suggesting the presence

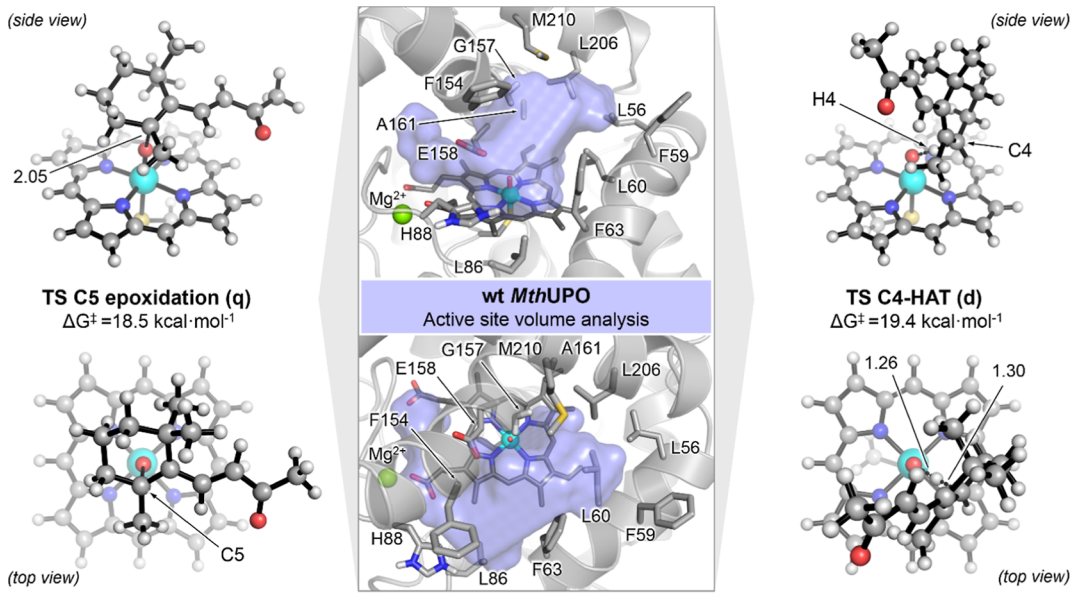


**Figure 2.** (Center) Characterized active site cavity of wt *Mth*UPO from *holo* state MD simulations. Representative structure of the most populated cluster (estimated form backbone RMSD analysis) obtained from five independent replicas of 1000 ns MD trajectories each (total of 5000 ns of accumulated simulation time).[14] DFT optimized, lowest in energy, TS geometries for: (Right) C4−H hydrogen atom transfer; and (Left) C5−C6 epoxidation. See Figures 1 and S2 for additional details. Energies are given in kcal·mol$^{-1}$, and key distances in Å. *β*-Ionone could easily bind in the available space in the active site in a catalytically relevant binding mode that resembles the NAC required for C4−H activation, but not for C5−C6 epoxidation. This is due to steric requirements and the shape of the active site cavity.



https://doi.org/10.1021/acscatal.3c00702
ACS Catal. 2023, 13, 8963−8972

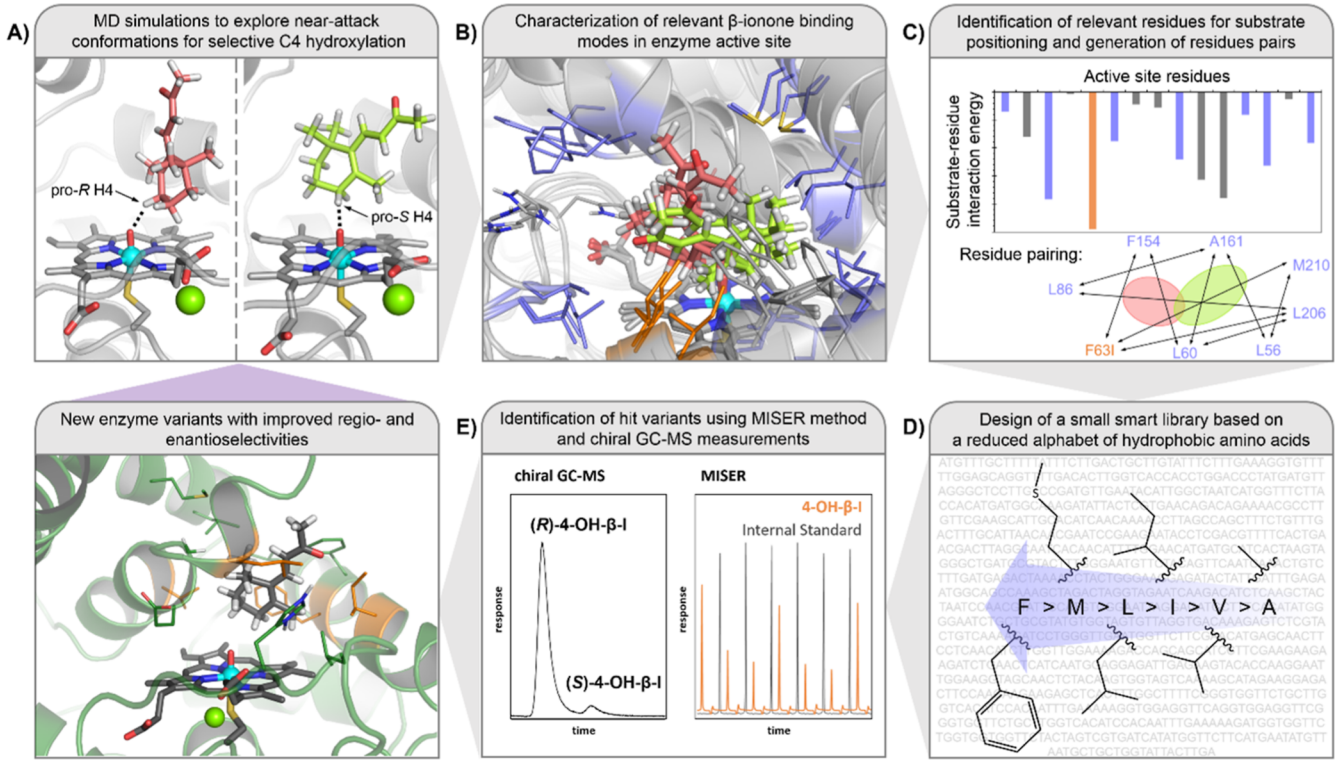


**Figure 3.** Schematic description of the computational-aided protein engineering protocol followed in this work. Red and green circles represent *β*-I substrate when bound in the active site cavity within different conformations. Complete descriptions of position selection for rounds 1 and 2 of protein engineering can be found in Figures S8 and S10, respectively.

of these incipient catalytically relevant binding modes that have yet to be fully exploited.

These simulations further revealed which active site amino acids exhibit strong interactions with the substrate, thus, affecting its binding mode. We reasoned that selecting positions as mutagenic spots that show strong steric interactions with the substrate during these restrained-MD simulations would give access to new variants with reshaped active sites. These new active sites are expected to better accommodate *β*-ionone in desired reactive conformations due to complementarity while destabilizing other alternative binding modes, thus inducing a shift in both regio- and enantioselectivity (Figure 3C). Following this reasoning, a total of eight positions (L56, L60, F63I, L86, F154, A161, L206, and M210) were initially selected based on restrained-MD analysis (Figure S8) and estimated substrate−residue interactions (estimated from MM-GBSA calculations, Figure S7). Amino acid positions that were determined to have a key role in proper substrate positioning (G157) or in $H_2O_2$ activation (H88 and E158) were not considered for mutagenesis.

Because targeted active site reshaping for enantioselectivity shifts might involve the reorientation of the substrate in the catalytic pocket, we hypothesized that mutating pairs of residues at the same time might facilitate this substrate reorientation due to cooperative effects.[39] Cooperativity, i.e., epistasis, between residue pairs can occur through direct interaction between residues but often also between distal indirect interactions.[40] These potential cooperative non-additive effects would be considered by including amino acid pairs for double saturation mutagenesis instead of saturation of single positions at a time.[36,41] We, hence, designed a set of 10 residue-pairs of proximal and—in terms of active site arrangement—also distal amino acid pairs combining previously selected active site residues (Figures 3C, a complete description of position selection can be found in Figure S8).

The *Mth*UPO active site is mainly composed of hydrophobic amino acids. The hydrophobic character was kept by employing a reduced amino acid alphabet consisting of Ala, Leu, Ile, Val, and Phe. For position M210, Met was also included (Figure 3D). This also reduces the number of possible variants for each double-saturation screening down to 25 (30 if position M210 is included). The screening is performed with a 3.5-fold oversampling leading to a library coverage of 97%. Inclusion of position M210 results in a 2.9-fold oversampling and 94% coverage.[42]

The screening was carried out in 96-well microtiter plates using the multiple injection in a single experimental run (MISER) (Figure 3E) setup,[14,16] allowing the determination of enzyme variant's activity but not its enantioselectivity. We reasoned that reshaping the active site results in an increased activity and simultaneously affects their enantioselectivity, as demonstrated multiple times before.[43]

**Development of Enantiodivergent *Mth*UPO Variants in Two Rounds of Directed Evolution.** In the first round, ten different double saturation pairs were screened (Table S5), adding up to more than 900 variants. The best variants showed increased activities of 2.0-fold under screening conditions compared to the parental variant *Mth*UPO F63I (Figure S15). With this first focused protein library, already impressive enantioselectivity improvements were detected (Table 1).

The best for the (*R*)-enantiomer formation showed an e.r. of 96.6:3.4 and a 4.3-fold improved activity of 28,000 TONs (*Mth*UPO F63I, L206A, coined R1A, Figure 4). In the same relatively small library, variants with inverted enantioselectivity


https://doi.org/10.1021/acscatal.3c00702
ACS Catal. 2023, 13, 8963−8972

**Table 1. Enantioselectivity after One Round of Protein Engineering**

| entry | new mutations | e.r. |
|---|---|---|
| *Mth*UPO F63I (parent) | | 70.7:29.3 |
| 1 | L206A | 96.6:3.4 |
| 2 | I63L, L206A | 95.2:4.8 |
| 3 | L56I, M210F | 85.2:14.8 |
| 4 | L206F | 82.0:18.0 |
| 5 | I63L, L206F | 81.3:18.8 |
| 6 | L206V | 80.5:19.5 |
| 7 | L56I, M210 | 79.5:20.5 |
| 8 | L56V, A161I | 29.4:70.6 |
| 9 | I63V, F154I | 12.0:88.0 |
| 10 | L60F, A161I | 11.5:88.5 |
| 11 | I63V, F154L | 7.3:92.7 |
| 12 | L60F, A161V | 3.3:96.7 |

could also be identified. The best showed an e.r. of 3.3:96.7 for the *S*-enantiomer and 20,000 TONs (*Mth*UPO L60F, F63I A161V, coined R1B).

Both variants were selected as parental variants for a second round of directed evolution (Figure S21).

Building upon the methodology established in the first iteration, we performed similar computational modeling. MD simulations, in this case without any restrain on $\beta$-ionone, were carried out to characterize and analyze the variants R1A and R1B (Figures S9 and S11). These simulations were used to design pairs of residues for library construction and subsequent screening, following the above-described protocol (Figures 3, S10, and S12).

In the second round, ten different double saturation pairs were screened with the parental variant R1A and eight different double saturation pairs with the parental variant R1B (Tables S6 and S7). The best variants based on R1A showed only a marginal increase in activity and no improved enantioselectivity. Based on these observations, we concluded that the evolutionary pathway had come to a local minimum and identified the best variant for (*R*)-4-hydroxy-$\beta$-ionone formation as *Mth*UPO F63I, L206A (R1A). This variant showed a high TON of 28,000 and an enantiomeric ratio of 96.6:3.4.

The best variant based on the *S*-selective variant R1B, however, displayed a substantial improvement. *Mth*UPO L60F, F63I, A161V, and F154L (R2B) displayed a 2.0-fold activity improvement to a TON of 41,000 and an e.r. of 99.7:0.3 (Figures 4 and S15, Table 2). The regioselective abundance of the main product also increased during the enzyme engineering campaign from 88% (*Mth*UPO wt expressed in *Saccharomyces cerevisiae*) to 99.2% (R1A) and 99.6% (R2B) (Table S9).

**Table 2. Enantioselectivity after Round 2B of Protein Engineering**

| entry | new mutations | e.r. |
|---|---|---|
| *Mth*UPO L60F, F63I, A161V (parent) | | 3.3:96.7 |
| 1 | F154L | 0.3:99.7 |
| 2 | F154I | 0.5:99.5 |
| 3 | F154V | 0.4:99.6 |
| 4 | F154I, M210L | 0.5:99.5 |
| 5 | F154L, M210L | 0.4:99.6 |

With the best engineered variant in hand, we repeated the enzymatic reactions in a scale-up experiment to give access to larger amounts of the hydroxylated product and demonstrate its utility. We were able to obtain 34 mg of (*S*)-4-hydroxy-$\beta$-ionone (55%)-utilizing variant, R2B, as a catalyst. We further obtained 51.1 mg (*R*)-4-acetoxy-$\beta$-ionone (37.0%) after hydroxylation of the substrate through variant R1A and subsequent derivatization to determine the specific optical rotation.

Both enzyme variants were purified and their transition temperature ($T_M$) determined (Table S13). Both variants showed a decreased transition temperature from initial 58.1 °C (wt MthUPO) to 53.7 °C (R1A) and 52.9 °C (R2B). To gain insights into the kinetics of the variants, the apparent catalytic parameters $K_m$ and $k_{cat}$ were determined for the substrate NBD (5-nitro-1,3-benzodioxole) and the co-substrate $H_2O_2$ (Table S14 and Figure S22). Both variants show an improved apparent $k_{cat}/K_m$ (1.9−4-fold) for both substrates relative to the wildtype (NBD: $1.9 \times 10^4$ $M^{-1}$ $s^{-1}$, $H_2O_2$: $1.3 \times 10^4$ $M^{-1}$ $s^{-1}$). Especially, variant R2B revealed a strong improvement of the apparent $k_{cat}$ toward both NBD (33.8 $s^{-1}$) and $H_2O_2$ (67.1 $s^{-1}$) in comparison with wt *Mth*UPO ($k_{cat}$ 7.1 $s^{-1}$). This is consistence with our previous work, demonstrating the beneficial influence of the mutations L60F and F63I for the NBD conversion.[14]

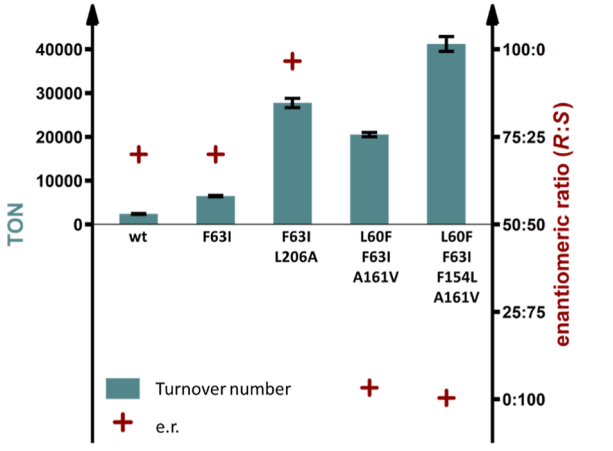


**Figure 4.** Bar chart showing TON within 1 h of allylic hydroxylation of $\beta$-ionone by different *Mth*UPO variants. Turnover data are mean ± s.d. of measurements in triplicates. TON (teal bars) determined by GC−MS, and enantiomeric excess (red cross) determined by chiral GC−MS (Figure S20).

**Molecular Basis of the Highly Enantioselective Variants R1A and R2B.** Finally, we performed computational modeling to rationalize the molecular basis for the enantiodivergence exhibited by R1A and R2B engineered variants. MD simulations with $\beta$-ionone bound in the active site of R1A and R2B—without including any geometric restraints during simulations—were carried out. MD simulations revealed the anticipated hydrophobic and steric interactions that control the binding modes for $\beta$-ionone and its orientation relative to the catalytically active Fe-oxo (Compound I) species.

MD simulations for R1A variant showed that $\beta$-ionone explores a major binding mode, in which only the pro-*R* C4−H is well oriented in a catalytically relevant NAC toward Compound I for HAT (Figures 5A and S9). This catalytically


https://doi.org/10.1021/acscatal.3c00702
ACS Catal. 2023, 13, 8963−8972

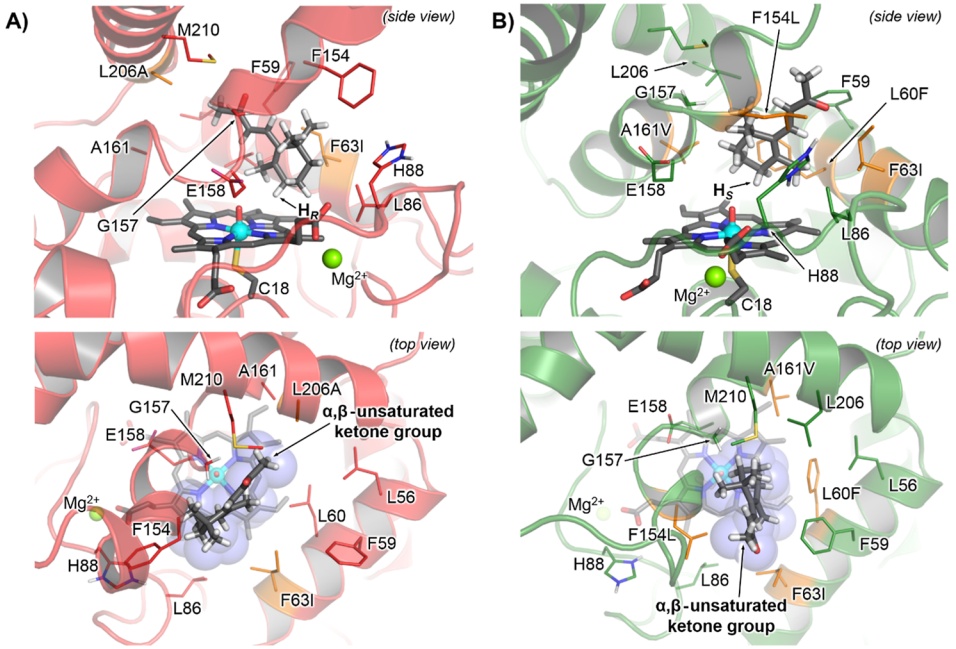


**Figure 5.** *β*-Ionone-binding modes characterized from MD simulations in (A) variant R1A (F63I/L206A, in red) and (B) variant R2B (L60F/F63I/F154L/A161V, in green). See Supporting Information for additional details.

relevant binding mode is stabilized due to the space generated by the initial F63I mutation, which is next to the region where C4 is oriented in the active site. The newly introduced L206A mutation reduces the steric hindrance, and it enables placing the *α,β*-unsaturated ketone group of the substrate and, thus, accommodating the *β*-ionone allylic chain in this region of the active site (Figure 5A). Within this favored binding mode of *β*-ionone, the pro-*R* C4−H bond is in a preorganized reactive conformation to promote a selective, pro-*R* HAT.

An opposite *β*-ionone positioning is observed in the R2B variant, where only the pro-*S* C4−H can explore reactive conformations relative to the Fe-oxo species (Figures 5B and S13). Unrestricted MD simulations revealed that when *β*-ionone is bound in R2B's active site, it preferentially explores a binding mode in which the *α,β*-unsaturated ketone group is oriented toward F154L position while keeping the six-membered ring in a similar position in the active site, as observed in R1A. This binding mode is favored by the A161V mutation that, together with the L206 residue, introduces bulkiness at this region of the active site. This sterically disfavors the positioning of the *α,β*-unsaturated ketone group in this area of the active site—contrary to R1A. The *α,β*-unsaturated ketone group is, thus, oriented toward the opposite side of the binding pocket where the F154L mutation is creating more empty space for accommodating this allylic substituent of *β*-ionone. The L60F mutation reduces the accessible space in that inner region of the active site, sterically disfavoring the positioning of the dimethyl and methyl *β*-ionone ring substituents there. All these factors synergistically favor the orientation of pro-*S* C4−H in a NAC toward the Fe-oxo species to selectively react via HAT.

These computational insights are in perfect agreement with the experimentally observed properties of the highly enantioselective variants, R1A and R2B.

## CONCLUSIONS

The presented work revealed the first substrate-targeted engineering of an UPO toward enantioselective C−H hydroxylation, starting from a poor enantioselectivity. Based on *in silico* predictions of the positioning for the substrate in the active site, excellent activities as well as regio- and enantioselectivities could be achieved by introducing very few mutations. In only two rounds of mutagenesis and the screening of 1600 variants, it was possible to evolve the wild-type *Mth*UPO with poor e.r. of 76:24 (*R*/*S*) toward the two enantiodivergent variants *Mth*UPO F63I, L206A (e.r. 96.6:3.4, (*R*)-selective) and *Mth*UPO L60F, F63I, F154L, A161V (e.r. 0.3:99.7, (*S*)-selective). In addition to high enantioselectivity, both variants also showed excellent regioselectivities with more than 99.2% and the activity increased up to 17-fold achieving TONs of 41,000.

The active site of *Mth*UPO seems to be particularly well-suited for selectivity engineering approaches due to its high hydrophobicity. This leads to two advantages: (i) significant high affinity toward different aliphatic substrates and (ii) the possibility of using a substantially reduced amino acid alphabet, exclusively consisting of hydrophobic amino acids, for active site reshaping while keeping the hydrophobicity and lowering the screening effort dramatically.

Further engineering of regio- and enantioselective functionalization of terpenes, terpenoids, linear- or branched hydrocarbon chains could be performed, similar to the presented work with the model substrate *β*-ionone.

Our MISER screening method based on GC−MS analysis offers a broad substrate flexibility, only limited to volatile, thermal stable molecules. This is an advantage in contrast to systems in which only chromogenic substrates can be examined. Even with the MISER approach, the screening remains the time-limiting factor; hence, the generation of a small smart library is still of utmost importance for reducing the overall engineering time. This is where the advantages


https://doi.org/10.1021/acscatal.3c00702
ACS Catal. 2023, 13, 8963−8972

offered by *in silico* analysis will be even more relevant in the future.

The present work paves the way toward the rapid engineering of UPOs for enantioselective conversion of terpene derivatives and other substrates and, hence, solves one of the last remaining challenges in UPO research.

## ■ ASSOCIATED CONTENT

### Supporting Information

The Supporting Information is available free of charge at https://pubs.acs.org/doi/10.1021/acscatal.3c00702.

Material and methods; computational methods and protocols; gene and protein sequence *Mth*UPO; energies, thermochemistry parameters and Cartesian coordinates of DFT optimized structures; oligonucleotides for cloning; initial screening data; saturation pairs for directed evolution campaign; TONs, regioselectivities and enantioselectivities for all variants; GC−MS parameters; chemical structures of all products; MD simulations and DFT calculations; screening data from directed evolution campaign; calibration curves; GC−MS chromatograms of non-chiral and chiral measurements; and NMR spectra (PDF)

## ■ AUTHOR INFORMATION


### Corresponding Authors

**Marc Garcia-Borràs** − *Institut de Química Computacional i Catàlisi and Departament de Química, Universitat de Girona, 17003 Girona, Catalonia, Spain;* orcid.org/0000-0001-9458-1114; Email: marc.garcia@udg.edu

**Martin J. Weissenborn** − *Department of Chemistry, Martin Luther-University Halle-Wittenberg, 06120 Halle (Saale), Germany; Leibniz Institute of Plant Biochemistry, 06120 Halle (Saale), Germany;* orcid.org/0000-0002-1200-4485; Email: martin.weissenborn@chemie.uni-halle.de

### Authors

**Judith Münch** − *Department of Chemistry, Martin Luther-University Halle-Wittenberg, 06120 Halle (Saale), Germany; Leibniz Institute of Plant Biochemistry, 06120 Halle (Saale), Germany*

**Jordi Soler** − *Institut de Química Computacional i Catàlisi and Departament de Química, Universitat de Girona, 17003 Girona, Catalonia, Spain*

**Nicole Hünecke** − *Department of Chemistry, Martin Luther-University Halle-Wittenberg, 06120 Halle (Saale), Germany*

**Dominik Homann** − *Department of Chemistry, Martin Luther-University Halle-Wittenberg, 06120 Halle (Saale), Germany; Leibniz Institute of Plant Biochemistry, 06120 Halle (Saale), Germany*

Complete contact information is available at: https://pubs.acs.org/10.1021/acscatal.3c00702


### Author Contributions

#J.M. and J.S. contributed equally. The manuscript was written through contributions of all authors. All authors have given approval to the final version of the manuscript.

### Notes

The authors declare no competing financial interest.

## ■ ACKNOWLEDGMENTS

J.M. thanks the Friedrich-Naumann-Stiftung für die Freiheit for a PhD scholarship. D.H. thanks the Friedrich-Ebert Stiftung for a PhD scholarship. M.J.W. and J.M. thank the Bundesministerium für Bildung und Forschung (Maßgeschneiderte Inhaltsstoffe 2, 031B0834A) and M.J.W., J.M., and D.H. thank the German Research Foundation (DFG, project ID 43649874, TP A05, RTG 2670) for generous funding. M.G.B. thanks the Spanish MICINN (Ministerio de Ciencia e Innovación) for PID2019-111300GA-I00 project and the Ramón y Cajal program via the RYC 2020-028628-I fellowship. J.S. thanks the Spanish MIU (Ministerio de Universidades) for a predoctoral FPU fellowship FPU18/02380. We would like to thank Dr. Franziska Seifert (Martin Luther University Halle-Wittenberg) for discussions and providing access to the DSF device for thermostability measurements.

## ■ ABBREVIATIONS

CAST, combinatorial active-site saturation test; DFT, density functional theory; GC−MS, gas chromatography−mass spectrometry; HAT, hydrogen-atom transfer; MD, Molecular Dynamics; MISER, multiple injection in a single chromatographical run for gas chromatography−mass spectrometry; NAC, near-attack conformation; $T_M$, transition temperature; TON, turnover number; TS, transition state; UPO, unspecific peroxygenase

## ■ REFERENCES


(1) (a) White, M. C.; Zhao, J. Aliphatic C−H oxidations for late-stage functionalization. *J. Am. Chem. Soc.* **2018**, *140*, 13988−14009. (b) Saint-Denis, T. G.; Zhu, R.-Y.; Chen, G.; Wu, Q.-F.; Yu, J.-Q. Enantioselective C (sp3)−H bond activation by chiral transition metal catalysts. *Science* **2018**, *359*, 6377. (c) Crabtree, R. H.; Lei, A. *Introduction: CH Activation*; ACS Publications, 2017; Vol. *117*, pp 8481−8482. (d) Chakrabarty, S.; Wang, Y.; Perkins, J. C.; Narayan, A. R. Scalable biocatalytic C−H oxyfunctionalization reactions. *Chem. Soc. Rev.* **2020**, *49*, 8137−8155.

(2) Chapman, J.; Ismail, A. E.; Dinu, C. Z. Industrial applications of enzymes: Recent advances, techniques, and outlooks. *Catalysts* **2018**, *8*, 238.

(3) Münch, J.; Püllmann, P.; Zhang, W.; Weissenborn, M. J. Enzymatic Hydroxylations of sp3-Carbons. *ACS Catal.* **2021**, *11*, 9168−9203.

(4) Urlacher, V. B.; Girhard, M. Cytochrome P450 monooxygenases in biotechnology and synthetic biology. *Trends Biotechnol.* **2019**, *37*, 882−897.

(5) (a) Beltrán-Nogal, A.; Sánchez-Moreno, I.; Méndez-Sánchez, D.; Gómez de Santos, P.; Hollmann, F.; Alcalde, M. Surfing the wave of oxyfunctionalization chemistry by engineering fungal unspecific peroxygenases. *Curr. Opin. Struct. Biol.* **2022**, *73*, 102342. (b) Wang, Y.; Lan, D.; Durrani, R.; Hollmann, F. Peroxygenases en route to becoming dream catalysts. What are the opportunities and challenges? *Curr. Opin. Chem. Biol.* **2017**, *37*, 1−9. (c) Molina-Espeja, P.; Santos, P. G. d.; Alcalde, M. Directed evolution of unspecific peroxygenase. In *Directed enzyme evolution: advances and applications*; Springer, 2017, pp 127−143.

(6) Hofrichter, M.; Kellner, H.; Pecyna, M. J.; Ullrich, R. Fungal unspecific peroxygenases: heme-thiolate proteins that combine peroxidase and cytochrome P450 properties. In *Monooxygenase, peroxidase and Peroxygenase properties and mechanisms of cytochrome P450*; Springer, 2015, pp 341−368.

(7) Molina-Espeja, P.; Garcia-Ruiz, E.; Gonzalez-Perez, D.; Ullrich, R.; Hofrichter, M.; Alcalde, M. Directed evolution of unspecific peroxygenase from Agrocybe aegerita. *Appl. Environ. Microbiol.* **2014**, *80*, 3496−3507.

(8) Püllmann, P.; Knorrscheidt, A.; Münch, J.; Palme, P. R.; Hoehenwarter, W.; Marillonnet, S.; Alcalde, M.; Westermann, B.; Weissenborn, M. J. A modular two yeast species secretion system for the production and preparative application of unspecific peroxygenases. *Commun. Biol.* **2021**, *4*, 562.
(9) Püllmann, P.; Weissenborn, M. J. Improving the heterologous production of fungal peroxygenases through an episomal Pichia pastoris promoter and signal peptide shuffling system. *ACS Synth. Biol.* **2021**, *10*, 1360−1372.
(10) Molina-Espeja, P.; Cañellas, M.; Plou, F. J.; Hofrichter, M.; Lucas, F.; Guallar, V.; Alcalde, M. Synthesis of 1-Naphthol by a Natural Peroxygenase Engineered by Directed Evolution. *ChemBioChem* **2016**, *17*, 341−349.
(11) Gomez de Santos, P.; Cañellas, M.; Tieves, F.; Younes, S. H.; Molina-Espeja, P.; Hofrichter, M.; Hollmann, F.; Guallar, V.; Alcalde, M. Selective synthesis of the human drug metabolite 5′-hydroxypropranolol by an evolved self-sufficient peroxygenase. *ACS Catal.* **2018**, *8*, 4789−4799.
(12) Martin-Diaz, J.; Paret, C.; García-Ruiz, E.; Molina-Espeja, P.; Alcalde, M. Shuffling the neutral drift of unspecific peroxygenase in Saccharomyces cerevisiae. *Appl. Environ. Microbiol.* **2018**, *84*, e00808−e00818.
(13) Gomez de Santos, P.; Hoang, M. D.; Kiebist, J.; Kellner, H.; Ullrich, R.; Scheibner, K.; Hofrichter, M.; Liers, C.; Alcalde, M. Functional expression of two unusual acidic peroxygenases from Candolleomyces aberdarensis in yeasts by adopting evolved secretion mutations. *Appl. Environ. Microbiol.* **2021**, *87*, No. e0087821.
(14) Knorrscheidt, A.; Soler, J.; Hünecke, N.; Püllmann, P.; Garcia-Borràs, M.; Weissenborn, M. J. Accessing Chemo-and Regioselective Benzylic and Aromatic Oxidations by Protein Engineering of an Unspecific Peroxygenase. *ACS Catal.* **2021**, *11*, 7327−7338.
(15) Carro, J.; González-Benjumea, A.; Fernández-Fueyo, E.; Aranda, C.; Guallar, V.; Gutiérrez, A.; Martínez, A. T. Modulating Fatty Acid Epoxidation vs Hydroxylation in a Fungal Peroxygenase. *ACS Catal.* **2019**, *9*, 6234−6242.
(16) Knorrscheidt, A.; Soler, J.; Hünecke, N.; Püllmann, P.; Garcia-Borràs, M.; Weissenborn, M. J. Simultaneous screening of multiple substrates with an unspecific peroxygenase enabled modified alkane and alkene oxyfunctionalisations. *Catal. Sci. Technol.* **2021**, *11*, 6058−6064.
(17) (a) González-Benjumea, A.; Linde, D.; Carro, J.; Ullrich, R.; Hofrichter, M.; Martínez, A. T.; Gutiérrez, A. Regioselective and stereoselective epoxidation of n-3 and n-6 fatty acids by fungal peroxygenases. *Antioxidants* **2021**, *10*, 1888. (b) Bassanini, I.; Ferrandi, E. E.; Vanoni, M.; Ottolina, G.; Riva, S.; Crotti, M.; Brenna, E.; Monti, D. Peroxygenase-Catalyzed Enantioselective Sulfoxidations. *Eur. J. Org. Chem.* **2017**, *2017*, 7186−7189. (c) Xu, X.; Paul, C.; Hollmann, F. Peroxygenase-catalysed enantioselective hydroxylation of ethylbenzene derivatives driven by formate oxidase. In *Expanding the Scope of $H_2O_2$-Driven Biocatalysis*; Doctoral Thesis; Delft University of Technology, 2022; p 99.
(18) Gomez de Santos, P.; Mateljak, I.; Hoang, M. D.; Fleishman, S. J.; Hollmann, F.; Alcalde, M. Repertoire of Computationally Designed Peroxygenases for Enantiodivergent C−H Oxyfunctionalization Reactions. *J. Am. Chem. Soc.* **2023**, *145*, 3443−3453.
(19) Christianson, D. W. Structural and chemical biology of terpenoid cyclases. *Chem. Rev.* **2017**, *117*, 11570−11648.
(20) Acevedo-Rocha, C. G.; Gamble, C. G.; Lonsdale, R.; Li, A.; Nett, N.; Hoebenreich, S.; Lingnau, J. B.; Wirtz, C.; Fares, C.; Hinrichs, H.; et al. P450-catalyzed regio-and diastereoselective steroid hydroxylation: efficient directed evolution enabled by mutability landscaping. *ACS Catal.* **2018**, *8*, 3395−3410.
(21) Le-Huu, P.; Heidt, T.; Claasen, B.; Laschat, S.; Urlacher, V. B. Chemo-regio-and stereoselective oxidation of the monocyclic diterpenoid β-cembrenediol by P450 BM3. *ACS Catal.* **2015**, *5*, 1772−1780.
(22) Beekwilder, J.; van Rossum, H. M.; Koopman, F.; Sonntag, F.; Buchhaupt, M.; Schrader, J.; Hall, R. D.; Bosch, D.; Pronk, J. T.; van Maris, A. J.; et al. Polycistronic expression of a β-carotene biosynthetic pathway in Saccharomyces cerevisiae coupled to β-ionone production. *J. Biotechnol.* **2014**, *192*, 383−392.
(23) Parker, G. L.; Smith, L. K.; Baxendale, I. R. Development of the industrial synthesis of vitamin A. *Tetrahedron* **2016**, *72*, 1645−1652.
(24) (a) Ansari, M.; Emami, S. β-Ionone and its analogs as promising anticancer agents. *Eur. J. Med. Chem.* **2016**, *123*, 141−154. (b) Aloum, L.; Alefishat, E.; Adem, A.; Petroianu, G. Ionone is more than a violet's fragrance: A review. *Molecules* **2020**, *25*, 5822.
(25) Luetragoon, T.; Pankla Sranujit, R.; Noysang, C.; Thongsri, Y.; Potup, P.; Suphrom, N.; Nuengchamnong, N.; Usuwanthim, K. Anti-Cancer effect of 3-Hydroxy-β-Ionone identified from moringa oleifera Lam. Leaf on human squamous cell carcinoma 15 cell line. *Molecules* **2020**, *25*, 3563.
(26) Wertz, P. W.; Kensler, T. W.; Mueller, G. C. Inhibition of phorbol ester action in lymphocytes by 5, 6-epoxy-β-ionone. *Biochem. Biophys. Res. Commun.* **1978**, *83*, 138−143.
(27) Zhou, J.; Geng, G.; Wu, J. H. Synthesis and in vitro characterization of ionone-based chalcones as novel antiandrogens effective against multiple clinically relevant androgen receptor mutants. *Invest. New Drugs* **2010**, *28*, 291−298.
(28) Babot, E. D.; Aranda, C.; del Río, J. C.; Ullrich, R.; Kiebist, J.; Scheibner, K.; Hofrichter, M.; Martínez, A. T.; Gutiérrez, A. Selective oxygenation of ionones and damascones by fungal peroxygenases. *J. Agric. Food Chem.* **2020**, *68*, 5375−5383.
(29) Urlacher, V. B.; Makhsumkhanov, A.; Schmid, R. D. Biotransformation of β-ionone by engineered cytochrome P450 BM-3. *Appl. Microbiol. Biotechnol.* **2006**, *70*, 53−59.
(30) Çelik, A.; Flitsch, S. L.; Turner, N. J. Efficient terpene hydroxylation catalysts based upon P450 enzymes derived from actinomycetes. *Org. Biomol. Chem.* **2005**, *3*, 2930−2934.
(31) Marumoto, S.; Shimizu, R.; Tanabe, G.; Okuno, Y.; Miyazawa, M. In Vitro Regio- and Stereoselective Oxidation of β-Ionone by Human Liver Microsomes. *Planta Med.* **2016**, *83*, 292−299.
(32) Kakeya, H.; Sugai, T.; Ohta, H. Biochemical preparation of optically active 4-hydroxy-β-ionone and its transformation to (S)-6-hydroxy-α-ionone. *Agric. Biol. Chem.* **1991**, *55*, 1873−1876.
(33) (a) Wijma, H. J.; Floor, R. J.; Bjelic, S.; Marrink, S. J.; Baker, D.; Janssen, D. B. Enantioselective enzymes by computational design and in silico screening. *Angew. Chem., Int. Ed.* **2015**, *54*, 3726−3730. (b) Cadet, F.; Fontaine, N.; Li, G.; Sanchis, J.; Ng Fuk Chong, M.; Pandjaitan, R.; Vetrivel, I.; Offmann, B.; Reetz, M. T. A machine learning approach for reliable prediction of amino acid interactions and its application in the directed evolution of enantioselective enzymes. *Sci. Rep.* **2018**, *8*, 16757−16815. (c) Li, G.; Dong, Y.; Reetz, M. T. Can machine learning revolutionize directed evolution of selective enzymes? *Adv. Synth. Catal.* **2019**, *361*, 2377−2386. (d) Rosales, A. R.; Wahlers, J.; Limé, E.; Meadows, R. E.; Leslie, K. W.; Savin, R.; Bell, F.; Hansen, E.; Helquist, P.; Munday, R. H.; et al. Rapid virtual screening of enantioselective catalysts using CatVS. *Nat. Catal.* **2018**, *2*, 41−45. (e) Romero-Rivera, A.; Garcia-Borràs, M.; Osuna, S. Computational tools for the evaluation of laboratory-engineered biocatalysts. *Chem. Commun.* **2017**, *53*, 284−297.
(34) Knorrscheidt, A.; Püllmann, P.; Schell, E.; Homann, D.; Freier, E.; Weissenborn, M. J. Identification of novel unspecific peroxygenase chimeras and unusual YfeX axial heme ligand by a versatile high-throughput GC-MS approach. *ChemCatChem* **2020**, *12*, 4788−4795.
(35) Reetz, M. T.; Wang, L. W.; Bocola, M. Directed evolution of enantioselective enzymes: iterative cycles of CASTing for probing protein-sequence space. *Angew. Chem., Int. Ed.* **2006**, *45*, 1236−1241.
(36) Reetz, M. T.; Bocola, M.; Carballeira, J. D.; Zha, D.; Vogel, A. Expanding the range of substrate acceptance of enzymes: combinatorial active-site saturation test. *Angew. Chem., Int. Ed.* **2005**, *44*, 4192−4196.
(37) (a) Acevedo-Rocha, C. G.; Hoebenreich, S.; Reetz, M. T. Iterative saturation mutagenesis: a powerful approach to engineer proteins by systematically simulating Darwinian evolution. In *Directed Evolution Library Creation*; Springer, 2014, pp 103−128. (b) Reetz, M. T.; Carballeira, J. D. Iterative saturation mutagenesis (ISM) for rapid


https://doi.org/10.1021/acscatal.3c00702
ACS Catal. 2023, 13, 8963−8972

directed evolution of functional enzymes. *Nat. Protoc.* **2007**, *2*, 891−903.
(38) Li, D.; Wu, Q.; Reetz, M. T. Focused rational iterative site-specific mutagenesis (FRISM). *Methods in Enzymology*; Elsevier, 2020; Vol. *643*, pp 225−242.
(39) (a) Acevedo-Rocha, C. G.; Li, A.; D'Amore, L.; Hoebenreich, S.; Sanchis, J.; Lubrano, P.; Ferla, M. P.; Garcia-Borràs, M.; Osuna, S.; Reetz, M. T. Pervasive cooperative mutational effects on multiple catalytic enzyme traits emerge via long-range conformational dynamics. *Nat. Commun.* **2021**, *12*, 1621. (b) Bocola, M.; Otte, N.; Jaeger, K. E.; Reetz, M. T.; Thiel, W. Learning from directed evolution: theoretical investigations into cooperative mutations in lipase enantioselectivity. *ChemBioChem* **2004**, *5*, 214−223. (c) Reetz, M. T.; Puls, M.; Carballeira, J. D.; Vogel, A.; Jaeger, K. E.; Eggert, T.; Thiel, W.; Bocola, M.; Otte, N. Learning from directed evolution: further lessons from theoretical investigations into cooperative mutations in lipase enantioselectivity. *ChemBioChem* **2007**, *8*, 106−112.
(40) Miton, C. M.; Tokuriki, N. How mutational epistasis impairs predictability in protein evolution and design. *Protein Sci.* **2016**, *25*, 1260−1272.
(41) Sun, Z.; Lonsdale, R.; Li, G.; Reetz, M. T. Comparing different strategies in directed evolution of enzyme stereoselectivity: single- versus double-code saturation mutagenesis. *ChemBioChem* **2016**, *17*, 1865−1872.
(42) Reetz, M. T.; Kahakeaw, D.; Lohmer, R. Addressing the numbers problem in directed evolution. *ChemBioChem* **2008**, *9*, 1797−1804.
(43) (a) van der Meer, J.-Y.; Poddar, H.; Baas, B.-J.; Miao, Y.; Rahimi, M.; Kunzendorf, A.; van Merkerk, R.; Tepper, P. G.; Geertsema, E. M.; Thunnissen, A.-M. W.; et al. Using mutability landscapes of a promiscuous tautomerase to guide the engineering of enantioselective Michaelases. *Nat. Commun.* **2016**, *7*, 10911−10916. (b) Zhang, D.; Chen, X.; Chi, J.; Feng, J.; Wu, Q.; Zhu, D. Semi−Rational engineering a carbonyl reductase for the enantioselective reduction of *β*-amino ketones. *ACS Catal.* **2015**, *5*, 2452−2457. (c) Chen, K.; Arnold, F. H. Engineering cytochrome P450s for enantioselective cyclopropenation of internal alkynes. *J. Am. Chem. Soc.* **2020**, *142*, 6891−6895.


https://doi.org/10.1021/acscatal.3c00702
*ACS Catal.* 2023, 13, 8963−8972